UNITED STATES DEPARTMENT OF THE INTERIOR

GEOLOGICAL SURVEY

Scattered Waves on the Wall of a Fluid-Filled Borehole From Incident Plane Waves

By M. W. Lee[1]

Open-File Report 85-666

[1]U.S. Geological Survey, Box 25046, Denver Federal Center, Denver, Colorado 80225

1985

CONTENTS

ILLUSTRATIONS

SCATTERED WAVES ON THE WALL OF A FLUID-FILLED BOREHOLE FROM INCIDENT PLANE WAVES

By M. W. Lee

ABSTRACT

The particle displacements from incident plane waves at the wall of a fluid-filled borehole were formulated by applying the seismic reciprocity theorem to far-field displacement fields due to point forces acting on a fluid-filled borehole under the long-wavelength assumption. The scattered wave fields were analyzed in order to examine the effect of the borehole on vertical seismic profiling (VSP) methods. This investigation demonstrated that when the shortest wavelength of interest is about 40 times longer than the borehole diameter, the borehole effect on VSP measurement using a wall-locking geophone is negligible.

INTRODUCTION

Most VSP data processing and interpretation are based on the assumption that seismic detectors were buried in the earth without disturbing or affecting the surrounding medium in any way. The extent to which data processing and interpretation are affected by the presence of a borehole and under what circumstances these effects are negligible are relevant to the development of VSP techniques. Therefore, it is important to know whether the waveforms recorded from a fluid-filled borehole by a wall-locking geophone are similar to the waveforms that would have been recorded in the absence of a borehole.

Balch and Lee (1984) showed that the presence of a fluid-filled borehole has a minimal effect on the vertical component of the particle displacement under the long-wavelength assumption. Blair (1984) discussed the effect of empty or fluid-filled boreholes on the incident P-wave in a two-dimensional medium. He showed that if the wavelength is greater than 30 times the borehole diameter, the borehole effect is negligible. However, if the wavelength is in the range of the borehole diameter or less, the borehole effect on seismic wave propagation can be substantial.

In order to investigate the influence of the borehole on seismic wave propagation, particle displacements at the wall of the borehole should be known. These displacement fields for incident plane waves at the wall of a fluid-filled borehole were derived by applying the seismic reciprocity theorem to the far-field displacement fields from point forces acting on the fluid-filled borehole. The required far-field displacement fields from the borehole sources were derived by Lee (1985) under the assumption that the wavelength of interest is much longer than the borehole diameter. Only scattered waves on the wall of the fluid-filled borehole are considered here. In this low-frequency range, the scattered field due to the borehole is proportional to a/λ, where λ is wavelength and a is the radius of the borehole. This study demonstrates that if the shortest wavelength of interest is about 40 times longer than the borehole diameter, the borehole effect on VSP measurement is insignificant.

DERIVATION OF DISPLACEMENT FIELDS

Assuming that a cylindrical borehole with a radius "a" is embedded in an isotropic, homogeneous, elastic medium with P-wave velocity α, S-wave velocity β, and density ρ, the fluid inside the borehole has a compressional velocity α_f and density ρ_f. If far-field displacement fields from point forces acting on the fluid-filled borehole are known, the displacement field at the wall of the fluid-filled borehole can be formulated by the seismic reciprocity theorem. White (1960) described the seismic reciprocity theorem as follows: "If, in a bounded, inhomogeneous, anisotropic, elastic medium, a transient force f(t) applied in some particular direction α at some point P creates at a second point Q a transient displacement whose component in some direction β is u(t), then the application of the same force f(t) at point Q in the direction β will cause a displacement at point P whose component in the direction α is u(t)."

Under the assumption that the wavelength of interest is very long compared to the borehole diameter, Lee (1985) derived far-field displacement fields in a spherical coordinate system (R, θ, $\emptyset$) from point forces acting on the wall of the fluid-filled borehole (fig. 1); the displacement component in R-, θ, and $\emptyset$-directions can be identified as P-, SH-, and SV-wave motion, respectively. The forces considered in Lee (1985) are directed in r-, θ-, and z-directions in a cylindrical coordinate system. Therefore, the particle displacements in r-, θ-, and z-directions on the wall of the fluid-filled borehole from the plane waves can be formulated by applying the seismic reciprocity theorem to the solutions derived by Lee (1985). For example, the radial displacement due to the incident SV-wave can be derived from the far-field displacement in the $\emptyset$ direction due to a force acting in the radial direction. More details of applying the seismic reciprocity theorem can be found in White (1960).

If $S(\omega)$ represents a Fourier-transformed, plane-wave displacement field, the displacements at the wall of the borehole from the plane waves can be written in the frequency domain as:

A. Incident P-wave:

$$U_r = S(\omega)\cos\theta\sin\phi + S(\omega)\frac{i\omega a}{\alpha}\left[\frac{T_\alpha(1-2\beta^2\cos^2\phi/\alpha^2)\alpha^2}{2i(T_\alpha+\rho_f/\rho)\beta^2} + \frac{\cos 2\theta\sin^2\phi}{(1-\beta^2/\alpha^2)}\right], \quad (1)$$

$$U_\theta = -S(\omega)\sin\theta\sin\phi - S(\omega)\frac{i\omega a}{\alpha}\frac{\sin 2\theta\sin^2\phi}{(1-\beta^2/\alpha^2)},$$

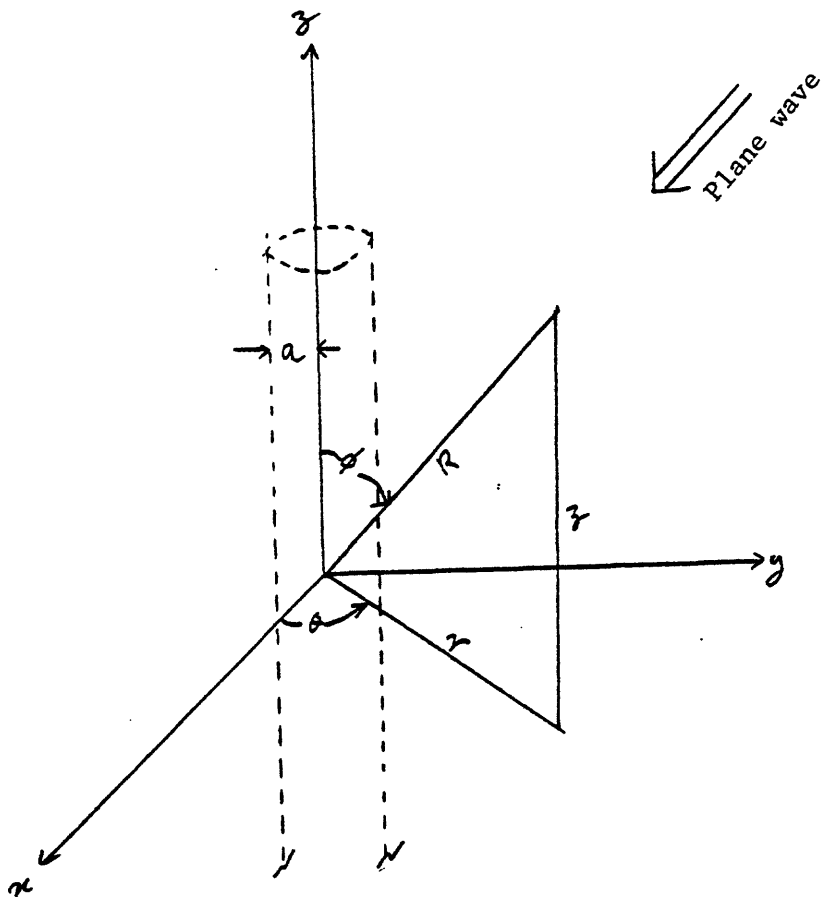

Figure 1.--Coordinate system for the analysis. An orthogonal Cartesian coordinate system (x, y, z), a cylindrical coordinate system (r, θ, z), and a spherical coordinate system (R, Ø, θ) are shown. Incident angles of plane waves are given by Ø.

$$U_3 = S(\omega)\cos\phi$$

$$+ S(\omega)\frac{i\omega a}{\alpha}\frac{3}{2}\cos\theta\sin 2\phi \,,$$

where

$$T_\alpha = \frac{\beta^2}{\alpha_f^2}\left(1 - \frac{\alpha_f^2\cos^2\phi}{\alpha^2}\right).$$

B. Incident SV-wave:

$$U_r = S(\omega)\cos\theta\cos\phi$$

$$+ S(\omega)\frac{i\omega a}{\beta}\left[\frac{T_\beta}{(T_\beta + \rho_f/\rho)} + \right. \tag{2}$$

$$\left. \frac{\cos 2\theta}{(1-\beta^2/\alpha^2)}\right]\frac{\sin 2\phi}{2} \,,$$

$$U_\theta = -S(\omega)\sin\theta\cos\phi$$

$$- S(\omega)\frac{i\omega a}{\beta}\frac{\sin 2\theta\sin 2\phi}{2(1-\beta^2/\alpha^2)} \,,$$

$$U_3 = -S(\omega)\sin\phi$$

$$- S(\omega)\frac{i\omega a}{\beta}\cos\theta\left(\sin^2\phi - \cos 2\phi\right) \,,$$

where

$$T_\beta = \frac{\beta^2}{\alpha_f^2}\left(1 - \frac{\alpha_f^2 \cos^2\phi}{\beta^2}\right).$$

C. Incident SH-wave:

$$U_r = S(\omega)\sin\theta + S(\omega)\frac{iwa}{\beta}\frac{\sin 2\theta \sin\phi}{(1-\beta^2/\alpha^2)}, \tag{3}$$

$$U_\theta = S(\omega)\cos\theta + S(\omega)\frac{iwa}{\beta}\left[\frac{1}{2} + \frac{\cos 2\theta}{(1-\beta^2/\alpha^2)}\right]\sin\phi,$$

$$U_z = S(\omega)\frac{iwa}{\beta}\sin\theta\cos\phi.$$

The terms proportional to $i\omega a$ in the equations (1), (2), and (3) denote the scattered waves from the borehole and the remaining terms represent the incident plane waves. Notice that when $a \longrightarrow 0$, the scattered displacement approaches 0.

The above displacement fields were derived based on the assumption that a is very small compared to the wavelength of interest. This assumption is very difficult to quantify unless higher order solutions are examined. However, based on the investigation by Greenfield (1978), it is assumed that if the smallest wavelength of interest is greater than 25 times the borehole diameter, the higher order solutions can be ignored. In other words, the displacement fields shown in equations (1), (2), and (3) are valid as long as the shortest wavelength of interest is in the order of 25 times longer than the borehole diameter.

For all of the following numerical analyses, a Poisson's solid is assumed.

DISCUSSION

Scattered Energy

The displacement fields shown in equations (1), (2), and (3) can be written as:

$$U_n^T(\omega) = U_n^I(\omega) + U_n^S(\omega),$$

where U_n^I, U_n^S, and U_n^T are the incident, scattered, and total displacement fields, respectively. Then, the energy partition between the incident and scattered waves can be defined as:

$$RE_1 \triangleq \frac{\sum_{n=1}^{3} \int U_n^S(\omega) \left[U_n^S(\omega)\right]^* d\omega}{\sum_{n=1}^{3} \int U_n^I(\omega) \left[U_n^I(\omega)\right]^* d\omega} \quad (4)$$

where * denotes a complex conjugate.

If the source function $S(\omega)$ is a band-limited signal and it has flat amplitude spectrum up to ω_m, then equation (4) becomes:

$$RE_1(\theta, \phi) = \frac{\omega_m^2 H^2(\theta, \phi)}{3}, \quad (5)$$

where H depends on the type of the incident plane waves. For example, when the incident plane wave is an SH-wave, H^2 can be written, from equation (3), as:

$$H^2 = \frac{a^2}{\beta^2} \sin^2\theta \cos^2\phi + \frac{a^2}{\beta^2} \sin^2\phi \left[\frac{1}{4} + \frac{1}{(1-\beta^2/\alpha^2)^2} + \frac{\cos^2\theta}{1-\beta^2/\alpha^2} \right].$$

As shown in equation (5), the amount of scattered energy depends not only on the frequency content of the source but also on the orientation of the geophone relative to the source.

Figure 2 shows the square root of RE_1 for the incident P-wave with respect to ϕ and the dimensionless parameter $(2a/\lambda_p)$ at $\theta = 0^o$, where λ_p is the shortest P-wave wavelength, and $\emptyset$ is the P-wave incident angle. The square root of RE_1, which is the amplitude ratio between incident and total displacement, is a linear function of ω_m or $2a/\lambda_p$. When $\emptyset = 90^o$ and $2a/\lambda_p = 0.04$, the scattered energy is about 4.5 percent of the incident wave; when $\emptyset = 0^o$, the scattered energy is less than 0.25 percent of the incident wave if $2a/\lambda_p < 0.04$.

For the incident SV-wave, the scattered energy is less than 2 percent of the incident energy at $\theta = 0^o$ when $\emptyset = 90^o$, and $2a/\lambda_s < 0.04$, where λ_s is the shortest S-wave wavelength; it reduces to about 0.4 percent when $\emptyset = 0^o$. For the incident SH-wave, the scattered energy is about 2 percent at $\theta = 0^o$, when $\emptyset = 90^o$, and $2a/\lambda_s = 0.04$; it reduces to zero when $\emptyset = 0^o$. For all incident waves, P-, SV-, or SH-waves, the maximum ratio of scattering energy to the incident energy occurs at $\emptyset = 90^o$ and $\theta = 0^o$, and is an increasing function of $\emptyset$.

Other useful information about scattered energy can be examined by the following formula.

$$RE_2(\phi) \triangleq \frac{\sum_{n=1}^{3} \int_0^{2\pi} \int_0^{\omega_m} U_n^S(\omega) \left[U_n^S(\omega)\right]^* d\omega\, d\theta}{\sum_{n=1}^{3} \int_0^{2\pi} \int_0^{\omega_m} U_n^I(\omega) \left[U_n^I(\omega)\right]^* d\omega\, d\theta} \quad . \tag{6}$$

RE_2 represents the "average" scattered energy with respect to the incident angle of the plane waves. Figure 3 shows the square root of RE_2 at $2a/\lambda_p = 0.04$ for P-wave, and $2a/\lambda_s = 0.04$ for SV- and SH-waves with respect to the incident angle of the plane wave.

Like RE_1, the maximum average scattered energy occurs at $\emptyset = 90^o$ for the incident P-wave, and it has about 2.5 percent of the incident energy when the shortest wavelength of interest is about 25 times the borehole diameter and it is about 1.3 percent or less for the S-waves.

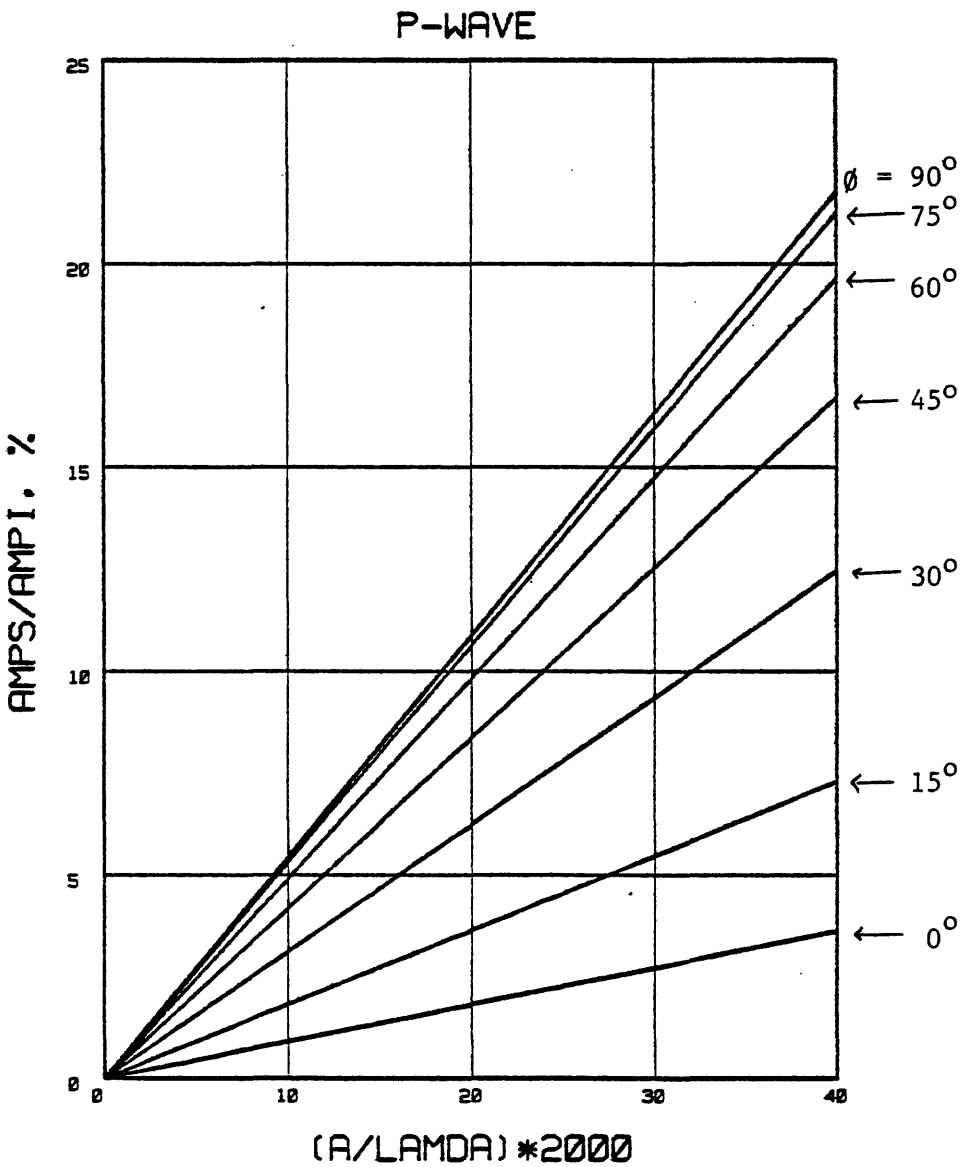

Figure 2.--Amplitude ratio of scattered and incident waves for the incoming P-wave at $\theta = 0^{\circ}$ with respect to dimensionless parameter $2a/\lambda$ and incident angle $\emptyset$ for an empty borehole.

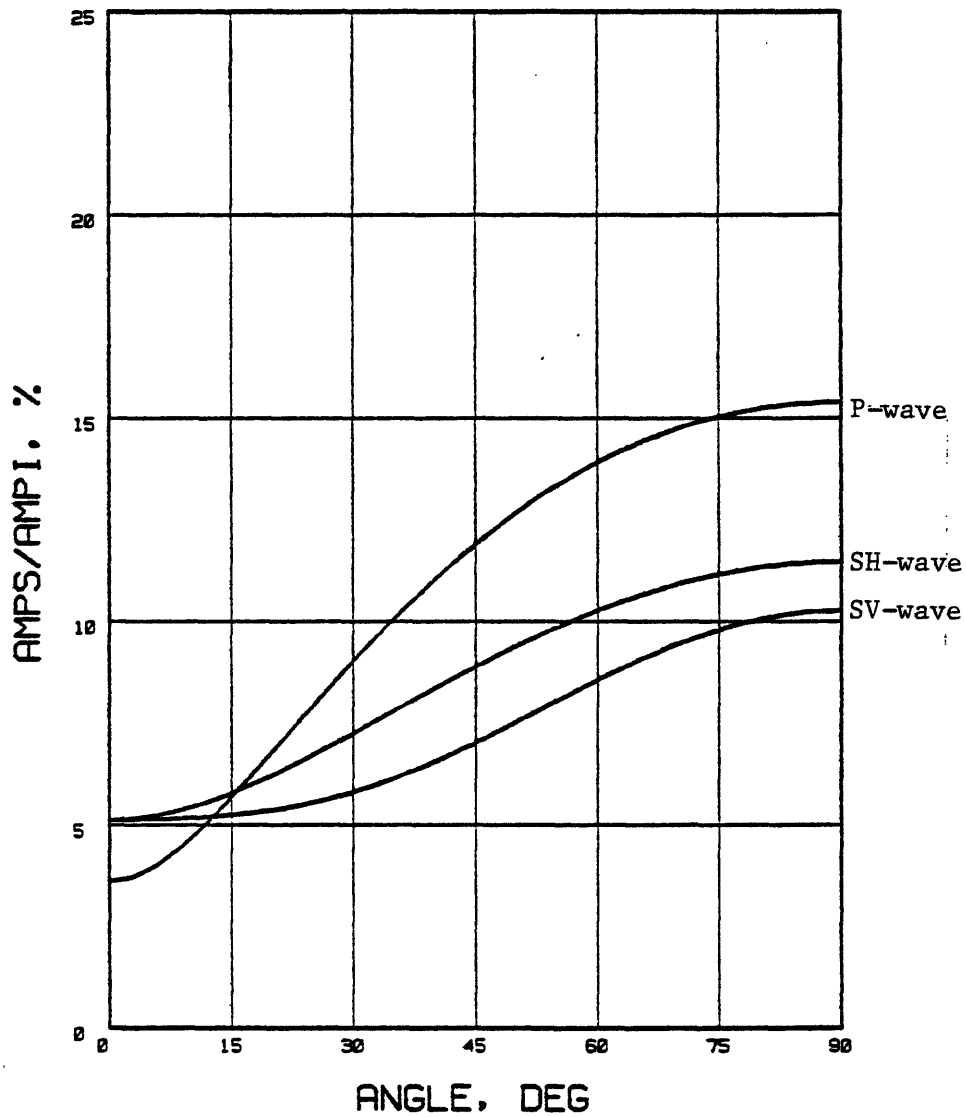

Figure 3.--Average amplitude ratio of scattered and incident waves with respect to the incident angle when the shortest wavelength of interest is 25 times longer than the borehole diameter for an empty borehole.

The fluid effect on the scattered wavefield is contained in the term $T_\beta/(T_\beta + \rho_f/\rho)$ for the incident SV-wave and $T_\alpha/(T_\alpha + \rho_f/\rho)$ for the incident P-wave. When there is no fluid in the borehole (an empty borehole), the above terms are equal to one. Because T_α or T_β is always a positive quantity, the scattered energy at the wall of the fluid-filled borehole is always less than the scattered energy at the wall of the empty borehole.

When a Ricker-type wavelet (characterized by a dominant or peak frequency instead of a flat amplitude spectrum) is used for the scattered energy analysis, the following relation can be derived from the Appendix:

$$\omega_m = \frac{\sqrt{15}}{2}\,\omega_p \cong 2\omega_p \tag{7}$$

where ω_p is the dominant frequency of the Ricker wavelet. By the relation shown in equation (7), the previous analysis for scattered energy can be applicable to the Ricker-type wavelet. For example, if the dominant wavelength is about 50 times larger than the borehole diameter, which is $2a/\lambda = 0.02$, the scattered energy is about 4 percent of the incident wave at $\theta = 0^\circ$ when $\phi = 60^\circ$, which is the value at $2a/\lambda = 0.04$ on figure 2.

Waveform Distortion

Equations (1), (2), and (3) indicate that the scattered waveform is the derivative of the incident waveform. Thus, the waveform of the measured displacement field at the borehole wall will differ from the incident wave, and the amount of waveform distortion depends on the frequency characteristic of the input wavelet. This distortion of the waveform can be regarded as amplitude and phase response of the transfer function, T_n, which is defined as:

$$T_n(\omega) \triangleq \frac{U_n^T(\omega)}{U_n^I(\omega)} \triangleq A_n(\omega)\, e^{i\phi_n(\omega)}. \tag{8}$$

where subscript n denotes the component of displacement. Notice that when $U_n^I(\omega) = 0$, the transfer function has no meaning.

These transfer functions represent the borehole effect on the incident plane waves. The transfer function of the vertical component displacement, T_z, for the incident P-wave can be written as:

$$A_3(\omega) = \left(1 + \frac{9\omega^2 a^2 \cos^2\theta \sin^2\phi}{\alpha^2}\right)^{1/2},$$

$$P_3(\omega) = \tan^{-1}\left(\frac{3\omega a \cos\theta \sin\phi}{\alpha}\right). \qquad (9)$$

When $\omega a/\alpha \ll 1$, then the phase spectrum can be approximated as:

$$P_3(\omega) \cong \frac{3\omega a \cos\theta \sin\phi}{\alpha}.$$

The linear approximation of the phase response for the long wavelength range implies the overall time delay or advance could be observed on the measured signal. The phase spectrum in equation (9), can be approximated by $\delta(t + \tau)$, where $\tau = 3a\cos\theta\sin\phi/\alpha$, in the time domain. The time delay or advance depends on the sign of τ. When $\theta = 0^\circ$, and $\phi = 90^\circ$, $\tau_0 = 3a/\alpha$. When $\theta = 180^\circ$ and $\phi = 90^\circ$, $\tau_{180} = -3a/\alpha$. Therefore, the arrival time in the direction of the source ($\theta = 0^\circ$) appears shorter than the arrival time in the opposite direction ($\theta = 180^\circ$). This example illustrates that the orientation of the downhole geophone could be important in certain cases. Greenfield (1978) observed similar P-wave arrival-time delays due to the cavity.

Figure 4 shows the transfer functions for the incident P-wave. The amplitude response of the transfer functions are shown in percent with solid lines, and the phase response in degrees by dotted lines with respect to $2a/\lambda_p$. The parameters for these transfer functions are: $\alpha/\alpha_f = 1.4$, $\rho/\rho_f = 2.2$. At $2a/\lambda_p = 0.04$, the amplitude response of T_r at $\theta = 0_o$ and $\phi = 90^\circ$ is about 0.3 db higher than the input function, and the phase is advanced by about 17 degrees. The transfer function concept can be easily illustrated by an example of the time-domain representation.

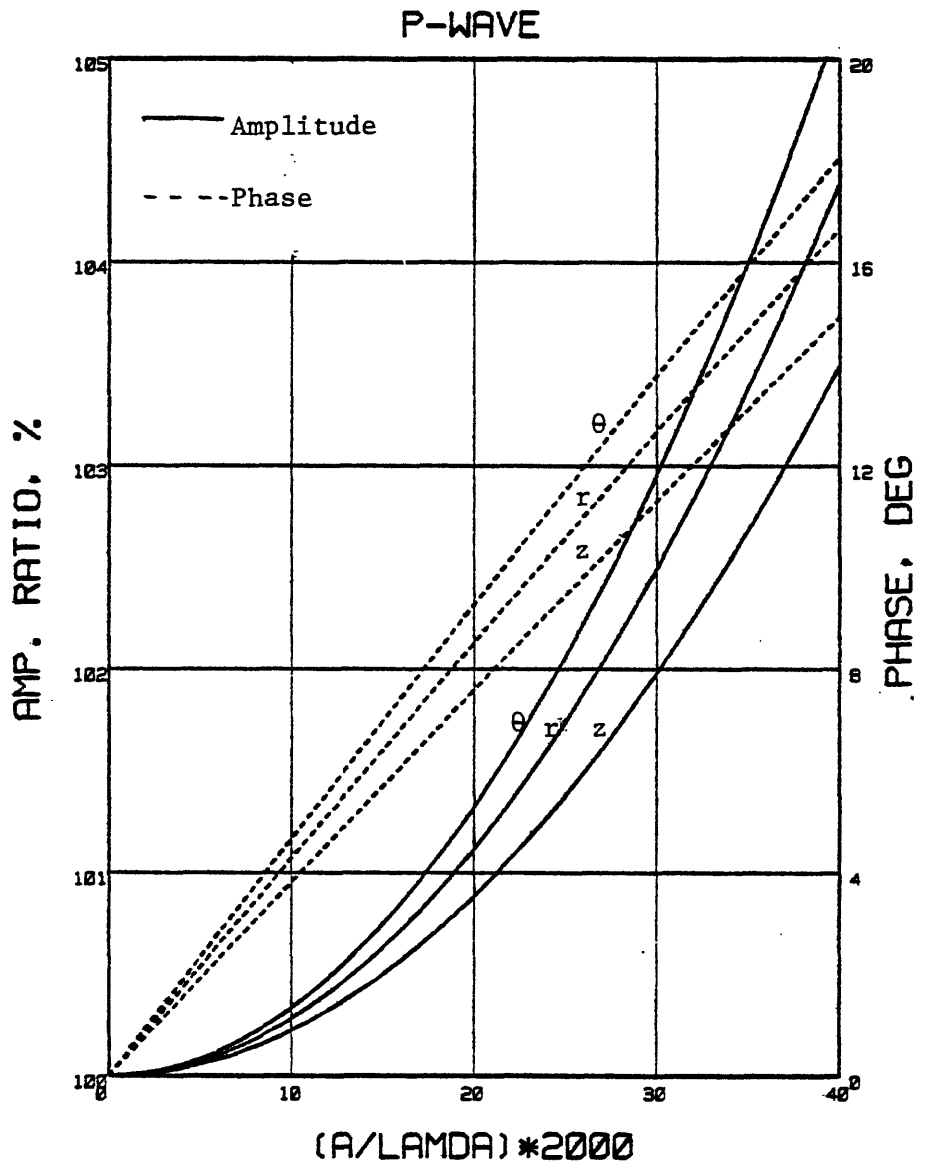

Figure 4.--Transfer functions for the incident P-wave with respect to $2a/\lambda$. Vertical component, T_z, is computed at $\theta = 0^\circ$ and $\phi = 45^\circ$, tangential component T_θ at $\theta = 30^\circ$ and $\phi = 90^\circ$; and the radial component at $\theta = 0^\circ$ and $\phi = 90^\circ$. Elastic parameters are: $\alpha/\alpha_f = 1.4$, $\rho/\rho_f = 2.2$, and $\alpha/\beta = \sqrt{3}$.

Figure 5 shows the time-domain response of the radial displacement for the incident P-wave in an empty borehole using 150 Hz Ricker wavelet with a = 0.2 m and α = 2,400 m/s. The solid heavy line represents the radial displacement at $\theta = 0^{\circ}$ and $\phi = 90^{\circ}$ in the absence of the borehole. The light solid line denotes the radial displacement at $\theta = 0^{\circ}$, which is in the direction of the source, and the light dotted line represents the radial displacement at $\theta = 180^{\circ}$ with a reverse polarity in an empty borehole.

The observed time difference ΔT = 0.5 ms is almost identical to the predicted value by $\Delta T = \tau_{180} - \tau_{0} = 6a/\alpha$. The maximum amplitude at $\theta = 0^{\circ}$ or $\theta = 180^{\circ}$ is about 4 percent higher than the input displacement. The slight distortion of the displacement due to the scattered energy can also be observed.

Figure 6 shows the incident, scattered, and total radial displacement field using 250 Hz Ricker wavelet for the incident P-wave with respect to the azimuthal angle when $\phi = 90^{\circ}$. The model parameters are: α = 2,000 m/s, $\alpha/\alpha_f = 1.4$, $\rho/\rho_f = 2.2$, a = 0.1 m. At the dominant wavelength, the transfer function shown in figure 4 predicts about 1.8 percent amplification of the amplitude and about 11° phase advance at $\theta = 0^{\circ}$. Notice that when $\theta = 90^{\circ}$, there are no incident waves. Thus, at $\theta = 90^{\circ}$, the displacement wholly consists of the scattered waves. In this instance, the transfer function concept has no meaning and cannot be applicable.

Some of the other transfer functions for SV- and SH-waves are shown in figures 7 and 8, respectively. The parameters for figures 7 and 8 are identical to those for figure 4.

Borehole Effect

Most VSP data are processed and interpreted based on the assumption that the seismic detectors were buried in the earth without any effect on the surrounding medium. In practice, of course, a borehole is required. How much the borehole disturbs or distorts the wavefield near the borehole is important not only from the theoretical point of view but also from the practical point of view. It is also very helpful to know the conditions under which borehole effects can be ignored on VSP measurements.

Most borehole effects were already considered in the previous section in the context of scattered fields. In this section, the effects of the borehole on seismic wave propagation around the borehole are considered in the context of data processing and interpretation.

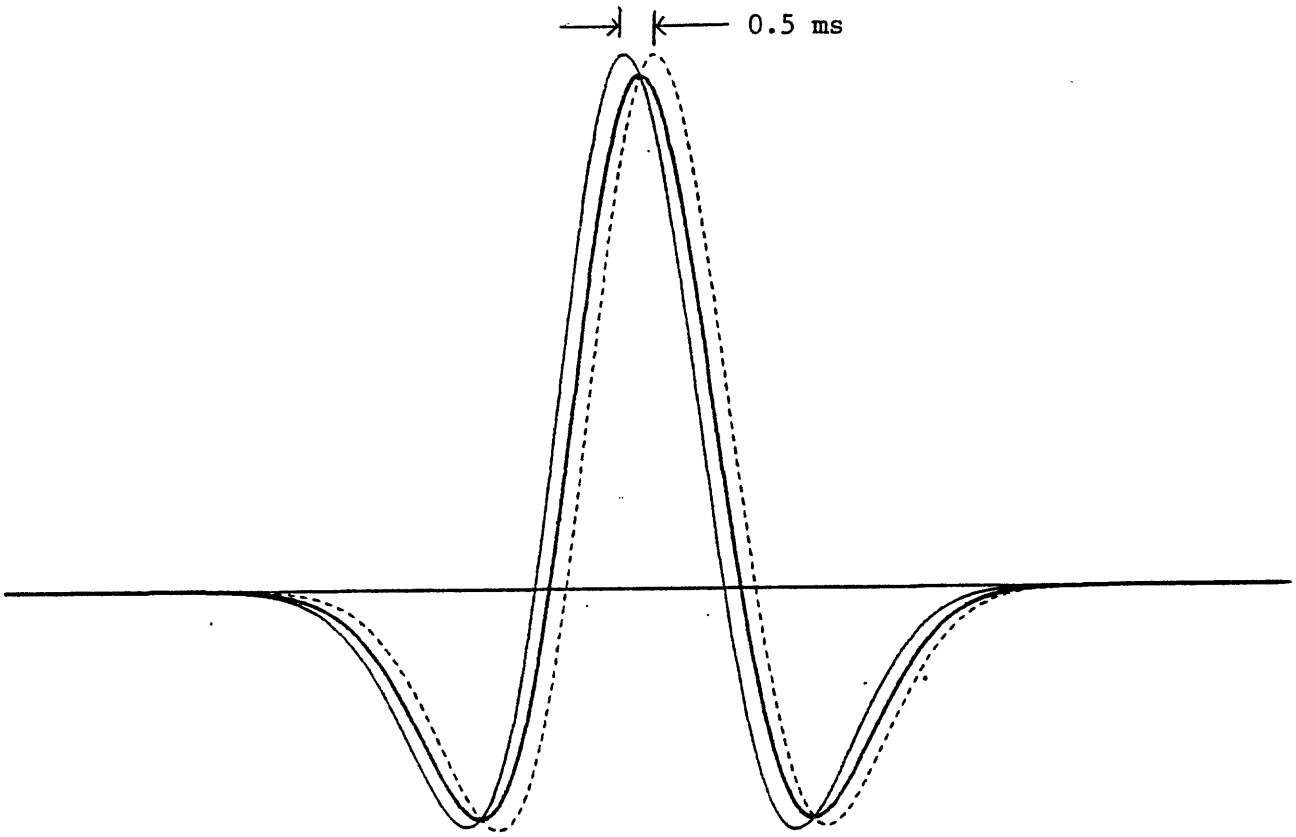

Figure 5.--Radial displacement at the wall of an empty borehole for the incident P-wave using 150 Hz Ricker wavelet. The heavy solid line represents the displacement in the absence of the borehole; the light solid line, $\theta = 0^{o}$ in the empty borehole; the light dotted line, $\theta = 180^{o}$ in an empty borehole with a reverse polarity. The parameters are: $a = 0.2$ m, $\alpha = 2{,}400$ m/s, and $\emptyset = 90^{o}$.

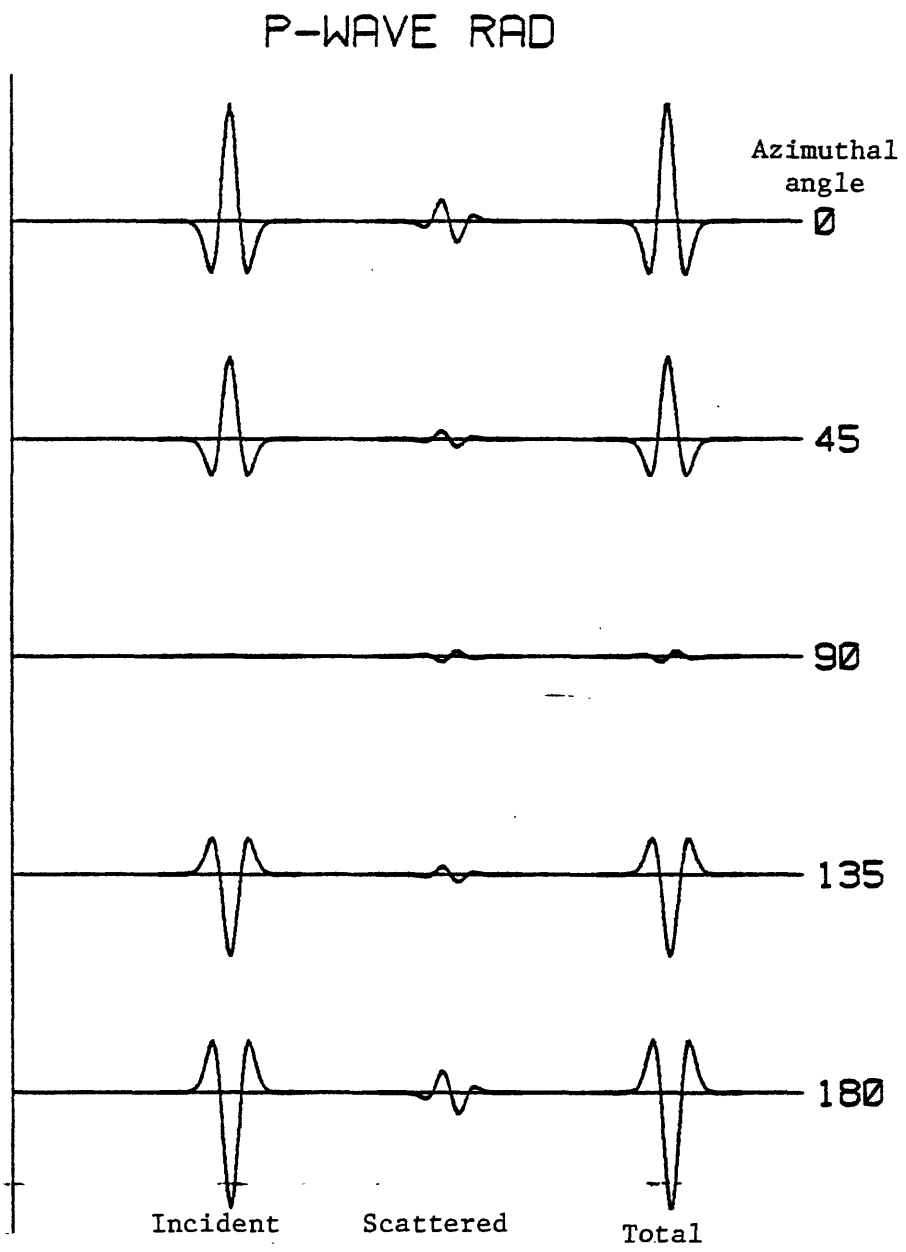

Figure 6. Radial displacement fields with respect to the azimuthal angle for the incident P-wave using 250 Hz Ricker wavelet in the fluid-filled borehole. Parameters are: α = 2,000 m/s, α/α_f = 1.4, ρ/ρ_f = 2.2, a = 0.1 m, and $\emptyset = 90^{\circ}$.

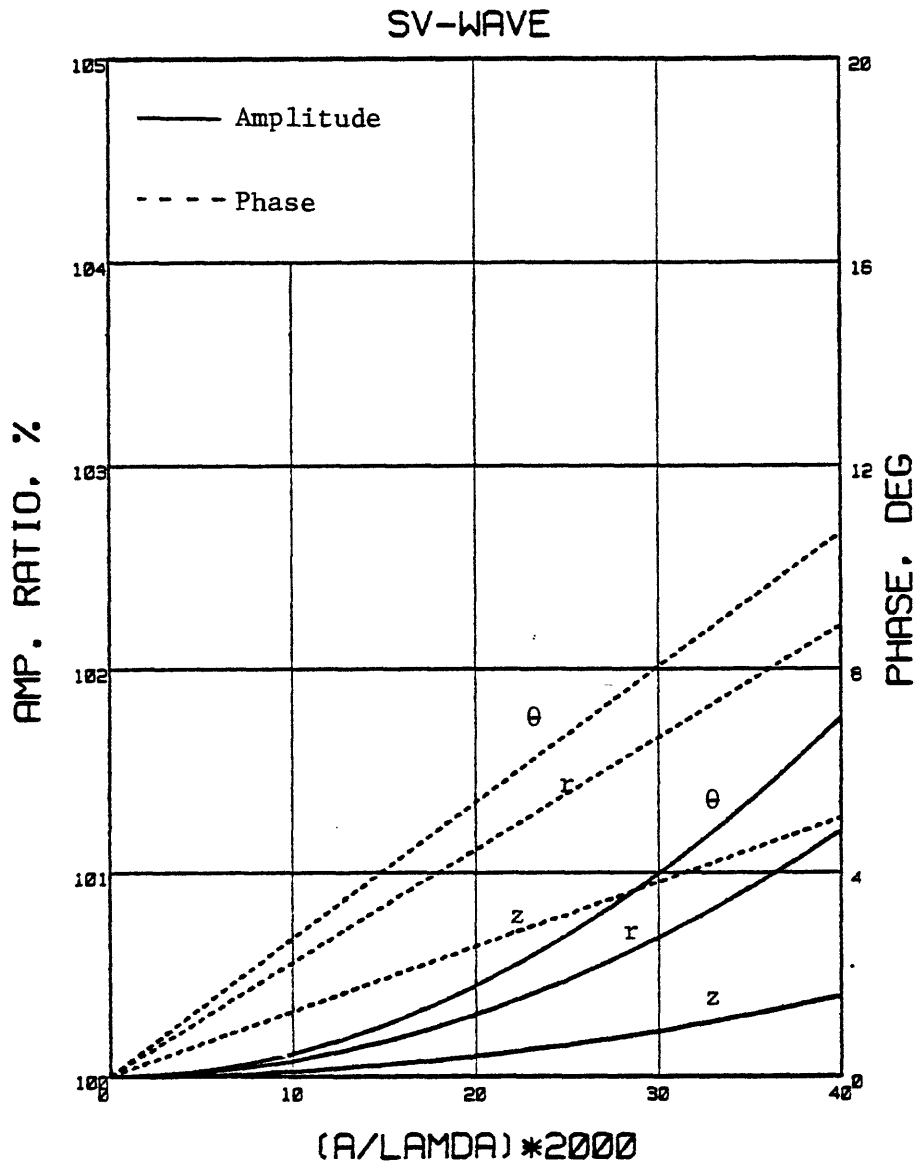

Figure 7.--Transfer functions for the incident SV-wave with respect to $2a/\lambda$. Vertical component, T_z, is computed at $\theta = 0^\circ$ and $\phi = 45^\circ$; tangential component, T_θ, at $\theta = 45^\circ$ and $\phi = 45^\circ$; and radial component, T_r at $\theta = 0^\circ$ and $\phi = 45^\circ$. Elastic parameters are: $\alpha/\alpha_f = 1.4$, $\rho/\rho_f = 2.2$, and $\alpha/\beta = \sqrt{3}$.

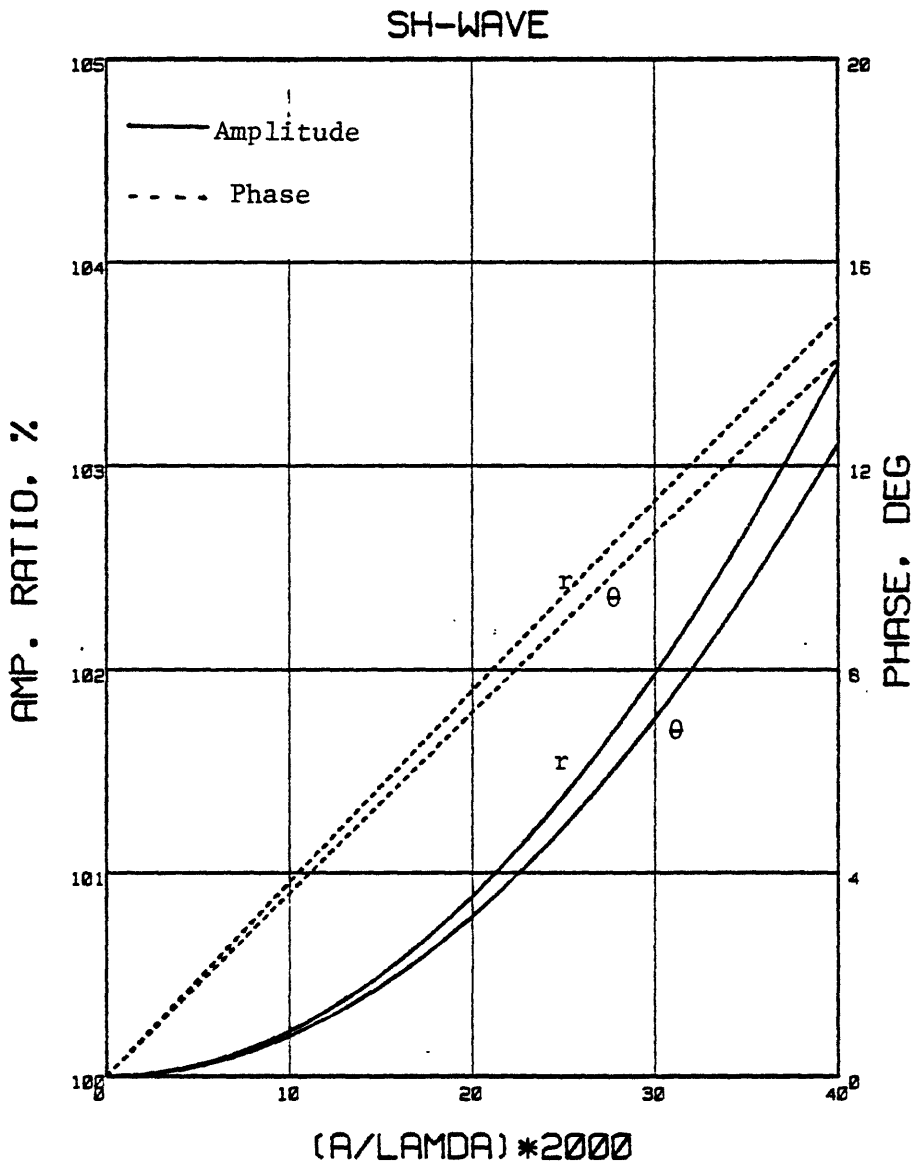

Figure 8.--Transfer functions for the incident SH-wave with respect to $2a/\lambda$. Tangential component, T_θ, is computed at $\theta = 0^\circ$ and $\phi = 90^\circ$; and radial component, T_r, at $\theta = 45^\circ$ and $\phi = 90^\circ$. Elastic parameters are: $\alpha/\alpha_f = 1.4$, $\rho/\rho_f = 2.2$, and $\alpha/\beta = \sqrt{3}$.

If the borehole detector can be oriented, the importance of the borehole effect on VSP processing and interpretation is greatly reduced. In this instance, borehole effects can be controlled by orienting the geophones in a certain azimuthal direction. For example, by orienting the geophone perpendicular to the incident P-wave, the effect of the borehole on the vertical component of displacement can be entirely removed. Therefore, in the following analysis, the orientation of the downhole geophone is assumed to be unknown and a random function of the geophone location in the hole.

The average scattered energy ratio (RE_2) in figure 3 shows that if the incident angle of the plane wave is less than 15^o, the scattered energy is less than 0.36 percent of the incident wave when the shortest wavelength of interest is about 25 times the borehole diameter. On the other hand, when the incident angle is 90^o, the scattered energy is about 2.5 percent of the incident wave. Thus, in conventional near-offset VSP measurement, the borehole effect may be negligible when $2a/\lambda \leq 0.04$. However, in hole-to-hole VSP configuration, or far-offset VSP, the effect of the borehole could be significant in some cases.

The effects of the borehole on VSP measurement can be addressed in many different ways using different criteria. Also, it is very subjective to state under which conditions borehole effects can be ignored. In this study, I assumed that if the maximum average scattered energy was less than 1 percent of the incident energy, the borehole effect on VSP measurement could be ignored. The validity of this assumption is examined in the following discussion.

The maximum average scattered energy due to the presence of the borehole occurs when $\phi = 90^o$ for the incident P-wave; it is less than 1 percent of the incident energy when $2a/\lambda < 0.025$. In the case of P-wave incidence, the radial displacement component contains the highest amount of the scattered energy and phase delay (or advance) at $\theta = 0^o$. Therefore, if the scattered radial displacement at $\theta = 0^o$ for the incident P-wave traveling perpendicular to the borehole ($\phi = 90^o$) can be ignored under certain criteria, then it can be also established that under the same criteria, borehole effects can be ignored on VSP measurements.

From equation (1), the amplitude and phase spectrum of the radial displacement on the empty borehole with a Poisson's solid can be written as:

$$A_r(\omega) = \left[1 + \frac{9\omega^2 a^2 (1 - 2\cos^2\phi/3 + \cos 2\theta \sin^2\phi)^2}{4\alpha^2 \cos^2\theta \sin^2\phi} \right]^{1/2}$$

$$P_r(\omega) = \tan^{-1} \left[\frac{3\omega a (1 - 2\cos^2\phi/3 + \cos 2\theta \sin^2\phi}{2\alpha \cos\theta \sin\phi} \right] \qquad (10)$$

As mentioned earlier, in the long-wavelength limit, the phase response can be approximated as a linear function of frequency; thus it can be represented as $\delta(t + \tau)$ with

$$\tau = \frac{3a (1 - 2\cos^2\phi/3 + \cos 2\theta \sin^2\phi)}{2\alpha \cos\theta \sin\phi}$$

in the time domain.

With $\phi = 90^{o}$, τ at $\theta = 0^{o}$ is given by $\tau_{0} = 3a/\alpha$. Therefore, the arrival time uncertainty due to the presence of the borehole would be in the range of $\Delta\tau = \pm 3a/\alpha$. The wavelength limit, $2a/\lambda < 0.025$, which was set for the criteria of the borehole effect, corresponds to $f_{m} \leq 0.0375\ \Delta\tau$, where f_{m} is the maximum frequency of interest. This implies that $\Delta\tau < 1/(25\ f_{m}) \simeq 1/(12\Delta t)$, where Δt is the sampling interval for the digital measurement. This analysis suggests that if the time uncertainty of $1/(12\Delta t)$ can be tolerated in the VSP measurement, the borehole effect on the arrival time can be ignored. Figure 9 shows the time-domain response of radial displacement using 150 Hz Ricker wavelet with α = 2,400 m/s, a = 0.1 m, which corresponds to $2a/\lambda$ = 0.025. The phase response predicts $\Delta\tau$ = 0.125 ms, which is very close to the numerical value shown in figure 9, and it is indeed less than $1/(12\Delta t)$.

The frequency-domain transfer function for the radial displacement is shown in figure 10, both for the empty and fluid-filled borehole. The parameters for the transfer function are identical to those for figure 4. The amplification of the peak amplitude due to the borehole in figure 9 is about 1 percent. The predicted amplification at the dominant wavelength shown on figure 10 is about 1 percent, which is close to the actual measurement on figure 9. If the waveform distortion or amplitude variation shown in figure 9 can be ignored, the borehole effect on amplitude and phase distortion can also be ignored.

The above analysis is based on the assumption that the orientation of the downhole geophone is unknown. If the data cannot be oriented by processing, the advantages obtained by three-component VSP measurement are greatly reduced. The orientation technique described by Lee (1984) assumed that the P-wave is plane-polarized and there is no borehole effect on the measurements. In the following, the degree of accuracy of the orientation of the geophone under influence of the borehole effect is discussed.

If X and Y are the observed horizontal components of the displacement field with an unknown orientation angle θ, then the unknown angle θ can be estimated by the following formula:

$$\tilde{\theta} = \frac{1}{2}\tan^{-1}\left[\frac{\int (XY^{*} + X^{*}Y)\,d\omega}{\int (YY^{*} - XX^{*})\,d\omega}\right] . \qquad (11)$$

Substituting U_{r} for X and U_{θ} for Y in equation (112), where U_{r} and U_{θ} are the radial and tangential components for the incident P-wave, the orientation angle θ is given by:

$$\tilde{\theta} = \frac{1}{2}\tan^{-1}\left[\tan 2\theta\left(1 + \frac{a^{2}\omega^{2}Q}{3\alpha^{2}}\right)\right] , \qquad (12)$$

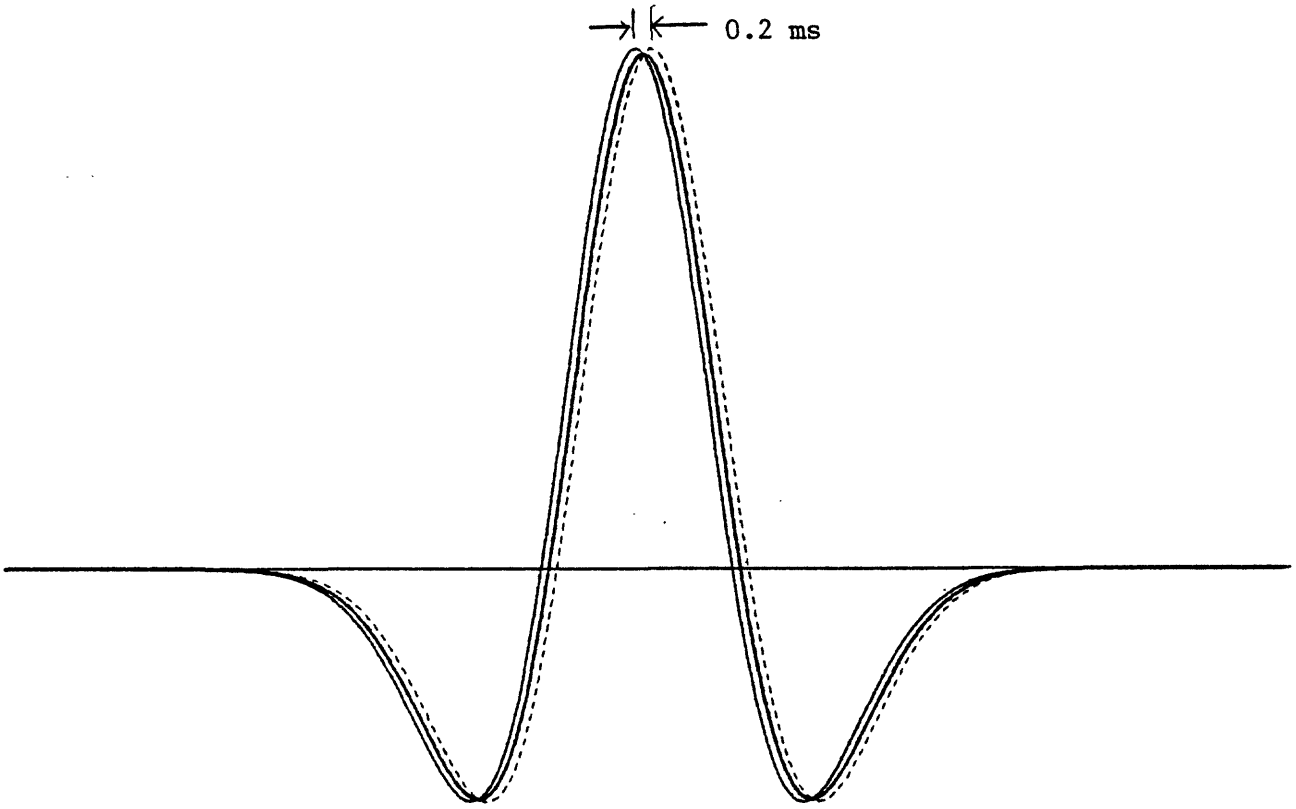

Figure 9.--Radial displacement at the wall of an empty borehole for the incident P-wave using 150 Hz Ricker wavelet. The heavy solid line represents the displacement in the absence of the borehole; the light solid line at $\theta = 0^{o}$ in the empty borehole; and the light dotted line at $\theta = 180^{o}$ in an empty borehole with a reverse polarity. The parameters are a = 0.1 m, α = 2,400 m/s, and $\emptyset = 90^{o}$.

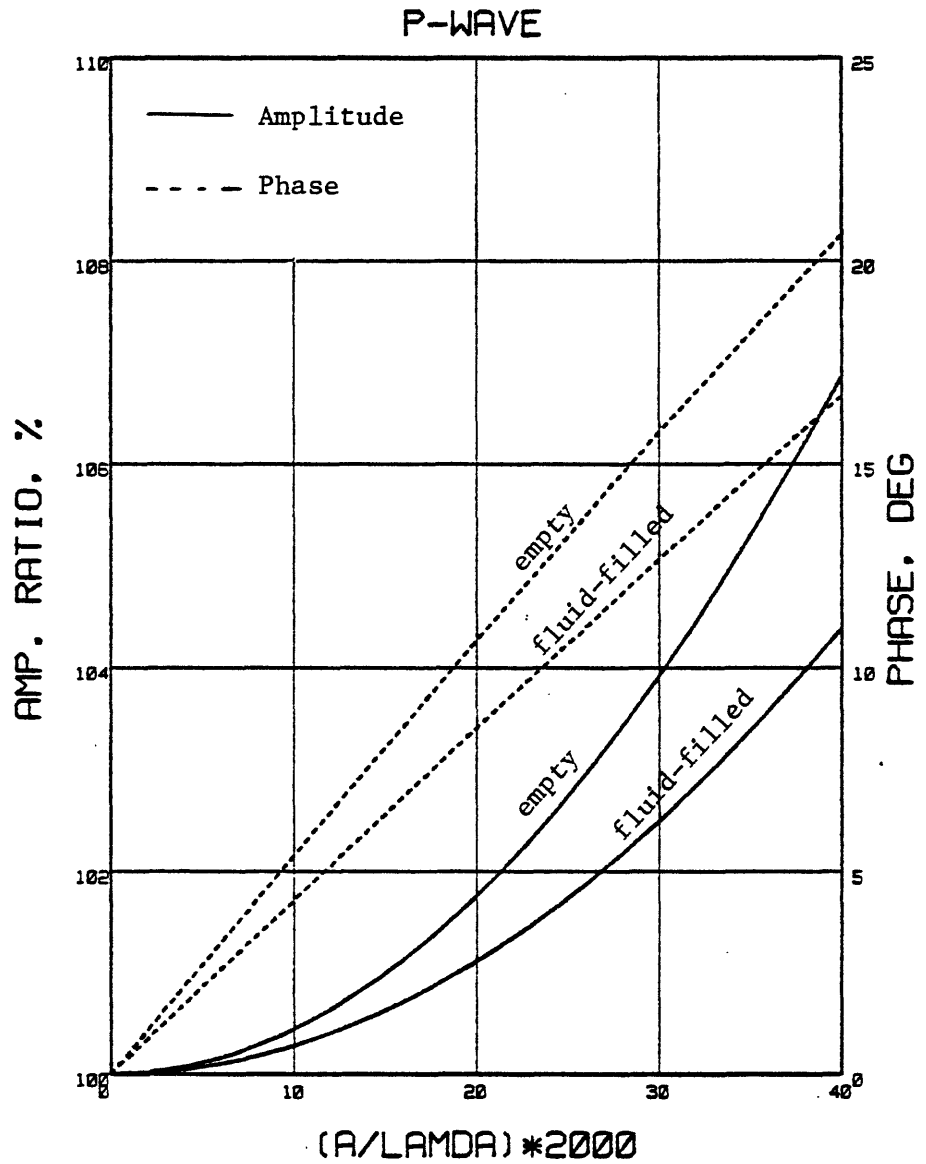

Figure 10.—Transfer functions of the radial displacement at $\theta = 0^{\circ}$ and $\phi = 90^{\circ}$ of the incident P-wave for the empty and fluid-filled borehole. Parameters are: $\alpha/\alpha_f = 1.4$, $\rho/\rho_f = 2.2$, and $\alpha/\beta = \sqrt{3}$.

where $$Q = -2(Q_1 + Q_2\cos 2\theta)/(1-\beta^2/\alpha^2) + \tan 2\theta \sin 2\theta \sin^2\phi/(1-\beta^2/\alpha^2)^2$$

$$- (Q_1 + Q_2\cos 2\theta)^2/\sin^2\phi\cos 2\theta,$$

$$Q_1 = \frac{\alpha^2}{2\beta^2}\,\frac{T_\alpha(1-2\beta^2\cos^2\phi/\alpha^2)}{(T_\alpha + P_+/\rho)}, \qquad Q_2 = \frac{\sin^2\phi}{(1-\beta^2/\alpha^2)}.$$

It is obvious from equation (12) that $a \longrightarrow 0$, and $\tilde{\theta} \longrightarrow \theta$.

Figure 11 shows the percentage error $\Delta\theta$, which is $\Delta\theta = (\theta - \tilde{\theta})/\theta$, when $\theta = 30^\circ$. When $2a/\lambda = 0.025$, the percentage error of the orientation is about 1 percent. Therefore, when the shortest wavelength of interest is about 40 times larger than the borehole diameter, the borehole effect on the orientation technique can be ignored.

CONCLUSIONS

The scattered wave fields at the wall of the fluid-filled borehole for incident plane waves were derived and then examined in order to determine the borehole effects on VSP measurement.

When plane waves propagate perpendicular to the borehole, the borehole has the most significant effect on seismic measurement; in certain cases, the orientation of the downhole geophone could be important. Thus the borehole effect could be more important in processing and interpreting the hole-to-hole VSP data and the upper section of far-offset VSP data. Furthermore, it has been shown that the scattered energy is less at the wall of a fluid-filled borehole than in an empty borehole.

If the shortest wavelength of interest is greater than 40 times the borehole diameter, or $2a/\lambda < 0.025$, then the following conclusions can be made on the VSP measurement:

1. The maximum average scattered energy is about 1 percent or less of the incident energy and occurs when the P-wave propagates perpendicular to the borehole axis.
2. The borehole effect on VSP measurements, such as arrival times and waveform distortion, can be negligible.
3. Controlling the orientation of the downhole geophone is desirable but not essential. The orientation technique based on plane polarization of the P-wave in the absence of a borehole can be applicable.

REFERENCES CITED

Balch, A. H., and Lee, M. W., 1984, Borehole seismology, in Balch, A. H., and Lee, M. W., eds., Vertical seismic profiling: Boston, International Human Resources Development Corporation, 488 p.

Blair, D. P., 1984, Rise times of attenuated seismic pulses detected in both empty and fluid-filled cylindrical boreholes: Geophysics, v. 49, p. 398-410.

Greenfield, R. J., 1978, Seismic radiation from a point source on the surface of a cylindrical cavity: Geophysics, v. 43, p. 1071-1082.

Lee, M. W., 1984, Processing of vertical seismic profile data, in Simaan, M., ed., Advances in geophysical data processing: Greenwich, JAI Press, Inc., v. 1, p. 129-160.

Lee, M. W., 1985, Two- and three-dimensional low-frequency radiation from an arbitrary source in a fluid-filled borehole: U.S. Geological Survey Open-File Report 85-550, 35 p.

White, J. E., 1960, Use of reciprocity theorem for computation of low-frequency radiation patterns: Geophysics, v. 25, p. 613-624.

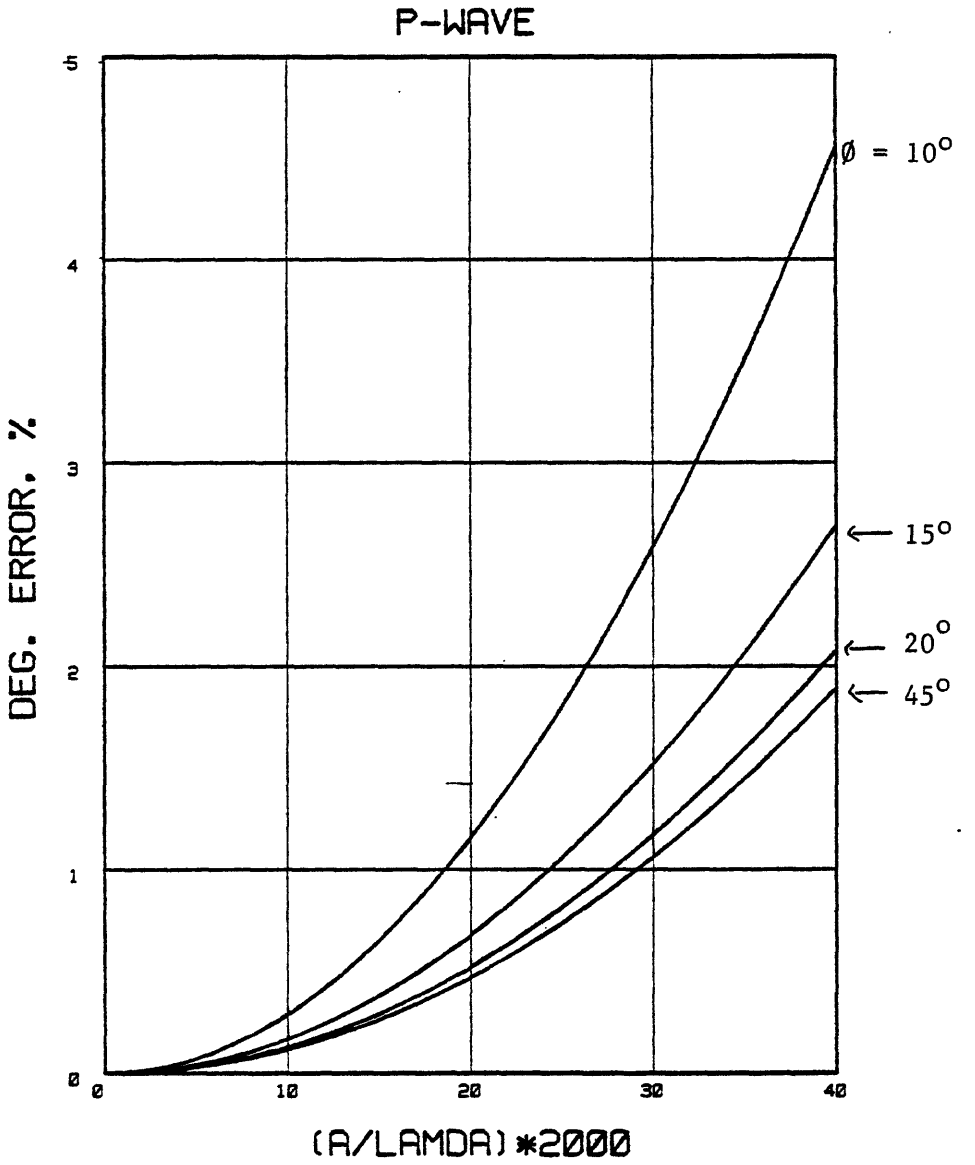

Figure 11.—Effect of an empty borehole on the orientation method for incident P-wave at $\theta = 30^{o}$ with respect to the incident angle.

APPENDIX

Derivation of equation (7):

$$\text{Let } (RE_1)^2 = \frac{\sum_{n=1}^{3} \int U_n^S \left[U_n^S\right]^* d\omega}{\sum_{n=1}^{3} \int U_n^I \left[U_n^I\right]^* d\omega}$$

$$= \frac{\int_0^{\omega_m} S(\omega) S^*(\omega) \omega^2 H^2(\theta,\phi)\, d\omega}{\int_0^{\omega_m} S(\omega) S^*(\omega)\, d\omega} \tag{A-1}$$

where $S(\omega)$ is the source waveform.

Let $S_1(\omega) = 1.0$ when $0 < \omega < \omega_m$

$= 0$ when $\omega > \omega_m$.

$$\text{Then } (RE_1^1)^2 \triangleq (RE_1)^2 \;\Big|\; S(\omega) = S_1(\omega) \tag{A-2}$$

$$= \frac{\omega_m^3}{3} H^2(\theta,\phi)$$

$$\text{Let's define } (RE_1^2)^2 \triangleq (RE_1)^2 \;\Big|\; S(\omega) = \text{Ricker wavelet.} \tag{A-3}$$

Ricker wavelet, r(t), can be defined in the time domain as:

$$r(t) = (1 - 2\alpha^2 t)\, e^{-\alpha t^2}$$

The Fourier transform of r(t) can be obtained by the following relation of g(t).

Let $g(t) = e^{-\alpha t}$;

then $g''(t) + 2\, g(t) = 4\alpha^2 g(t) t^2$.

Therefore, the Fourier transform of r(t), $R(\omega)$ can be written as:

$$R(\omega) = \frac{\omega^2}{2\alpha} G(\omega) \tag{A-4}$$

where $G(\omega)$ is the Fourier transform of $g(t)$, which is

$$G(\omega) = \sqrt{\frac{\pi}{\alpha}}\, e^{-\omega^2/4\alpha}$$

Substituting equation (A-4) into (A-3),

$$(RE_1^2)^2 = \frac{\int \omega^6 e^{-\omega^2/2\alpha}\, d\omega}{\int \omega^4 e^{-\omega^2/2\alpha}\, d\omega} \qquad \text{(A-5)}$$

Using the following relation,

$$\int_0^\infty \omega^{2n} e^{-\alpha\omega^2}\, d\omega = \frac{1 \cdot 3 \cdot \cdots \cdot (2n-1)}{2^n} \sqrt{\frac{\pi}{\alpha^{2n+1}}}$$

it can be shown that:

$$(RE_1^2)^2 = 5\alpha H^2, \text{ with} \qquad \text{(A-6)}$$

$$\alpha = \pi^2 f_p^2$$

where f_p is the dominant frequncy of the Ricker wavelet.

Equating (A-6) to (A-2) results in:

$$f_m = \frac{\sqrt{15}}{2} f_p \cong 2 f_p \quad \text{or} \qquad \text{(A-7)}$$

$$\omega_m \cong 2\omega_p .$$